Electrical and magnetic transport properties of Fe_3O_4 thin films on a GaAs(100) substrate

2007 J. Phys.: Condens. Matter 19 486212

(http://iopscience.iop.org/0953-8984/19/48/486212)

IOP PUBLISHING JOURNAL OF PHYSICS: CONDENSED MATTER

J. Phys.: Condens. Matter **19** (2007) 486212 (9pp) doi:10.1088/0953-8984/19/48/486212

Electrical and magnetic transport properties of Fe_3O_4 thin films on a GaAs(100) substrate

Ram Prakash[1], **R J Choudhary**[1], **L S Sharath Chandra**[1], **N Lakshmi**[2] **and D M Phase**[1,3]

[1] UGC-DAE Consortium for Scientific Research, University Campus Khandwa Road, Indore, MP-452017, India
[2] Department of Physics, M L Sukhadia University, Udiapur, 313001, India

E-mail: dmphase@csr.ernet.in

Received 27 June 2007
Published 13 November 2007
Online at stacks.iop.org/JPhysCM/19/486212

Abstract

Thin films of magnetite (Fe_3O_4) are grown on a single-crystal GaAs(100) substrate by pulsed laser deposition. The x-ray diffraction (XRD) result shows the (111) preferred orientation of the Fe_3O_4 film and x-ray photoelectron spectroscopy confirms the presence of single-phase Fe_3O_4 in the film. The electrical transport property of the film shows the characteristic Verwey transition at 122 K, and below 110 K the transport follows a variable range hopping type conduction mechanism. The film shows a room-temperature magnetization hysteresis loop, suggesting ferrimagnetic behavior of the film with a saturation magnetization value close to 470 emu cm^{-3}.

1. Introduction

Ever since magnetism in magnetite (Fe_3O_4) was discovered, the material has revolutionized the world of science with its fascinating properties. The material has been at the core of applications such as electric motors, electromagnets, transformers, video/audiotapes, magnetic inks, biomedical applications, etc. In recent years, there have been developments in storage devices such as hard disks, floppy disks, read heads, bubble memory, magnetic random access memory (MRAM), etc. The development of this field is attributed to the search for spintronic-based devices [1–3], wherein the spin-based transport properties of a material are exploited. Fe_3O_4 also falls under the category of such a functional material owing to its fascinating properties such as high Curie temperature (∼850 K), half metallicity, and low electrical resistivity at room temperature.

Fe_3O_4 is an inverse cubic spinel compound, wherein iron ions are shared between tetrahedral and octahedral sites; tetrahedral sites being occupied by Fe^{3+} ions whereas,

[3] Author to whom any correspondence should be addressed.

octahedral sites by both Fe^{3+} and Fe^{2+} ions in the same ratio. The magnetic interaction among iron ions at octahedral and tetrahedral sites is antiferromagnetic and that among octahedral ions is ferromagnetic; overall a ferrimagnetic arrangement of Fe_3O_4. Therefore, the net magnetic moment in Fe_3O_4 is due to Fe^{2+} ions (4 μ_B). Fe_3O_4 undergoes charge ordering at 120 K (known as the Verwey transition temperature, T_V) leading to an abrupt increase in its resistivity while cooling [4]. Across this temperature, structural transition also takes place from high-temperature cubic structure to low-temperature monoclinic structure. In spite of the evident spintronic potential of Fe_3O_4, it has not so far been optimized for its best functionality in the field. The crucial reason for this lack of its inclusion in device architectures is its poor control and the need for exploration of the growth of Fe_3O_4 films on technologically important semiconducting substrates like Si or GaAs. In this context, we attempt to study the nature of Fe_3O_4 thin films grown on GaAs substrates and compare it with the films grown on conventionally used MgO substrates for Fe_3O_4.

Thin films of magnetite have been prepared by a variety of deposition techniques such as molecular beam epitaxy (MBE), reactive magnetron sputtering, pulsed laser deposition. etc on different substrates such as MgO, $MgAl_2O_4$, α-Al_2O_3, $SrTiO_3$, Pt, Si, GaAs, etc [5–17] for their transport and magnetic properties. From these studies there is a consensus that the electrical transport properties *vis a vis* the magnetic properties of magnetite thin films are a function of the nature of defects (internal or external) and defect densities present in the film. From the available literature, we note that the growth of Fe_3O_4 films on GaAs substrate is not well explored, though it has huge potential in spintronic devices. Lu *et al* [12] employed electron beam evaporation to grow Fe_3O_4 films by initially growing Fe films on GaAs(100) followed by its oxidation. The procedure resulted in the epitaxial growth of magnetite on GaAs(100) with an epitaxial relation of $Fe_3O_4(100)\langle 011\rangle \parallel GaAs(100)\langle 010\rangle$. However, such a method limited the thickness of the film to 6 nm only. They also showed that the easy axis of magnetization is along the $[0\bar{1}\bar{1}]$ direction of the GaAs(100) substrate. Watts *et al* [13, 14] reported the (111) preferred oriented Fe_3O_4 thin film on GaAs(100) substrate but they detected the presence of some other orientations as well, such as (220), (311), (511), etc. Kennedy *et al* [15] reported (111) oriented magnetite film using an iron target for ablation in the presence of O_2 background by the Nd:YAG pulsed laser deposition technique. Unusually high magnetization (730 emu cm^{-3}) was observed in the film because of amorphous iron present in the film. From these studies it seems that a general agreement regarding the properties and the growth of Fe_3O_4 films on a GaAs substrate is yet to be achieved. In the present paper we study the structural, electrical, and magnetic transport properties of Fe_3O_4 thin films grown by the pulsed laser deposition technique on GaAs(100) substrates.

2. Experimental details

The thin films of Fe_3O_4 were grown on single-crystal GaAs(100) by the pulsed laser deposition (PLD) technique. The target used for the deposition is an α-Fe_2O_3 pallet prepared from high purity α-Fe_2O_3 powder, sintered at 950 °C for 24 h. Before ablation, surface contaminations were removed from the GaAs substrates using a H_2SO_4:H_2O_2:H_2O (4:1:1) solution etching for 30 s, with subsequent rinsing by de-ionized water and methanol cleaning. The cleaned substrate was mounted on a heater (substrate holder) and placed immediately in the deposition chamber, which was then evacuated to the base pressure of 2×10^{-6} Torr. During the ablation, the laser beam from a KrF excimer laser (wavelength 248 nm) was focused on to the target and its repetition rate was kept at 10 Hz. The laser energy density at the target was kept at 1.8 J cm^{-2} and the substrate temperature was maintained at 450 °C during deposition. The deposition was carried out for 20 min. The thickness of the film was 1500 Å, as measured

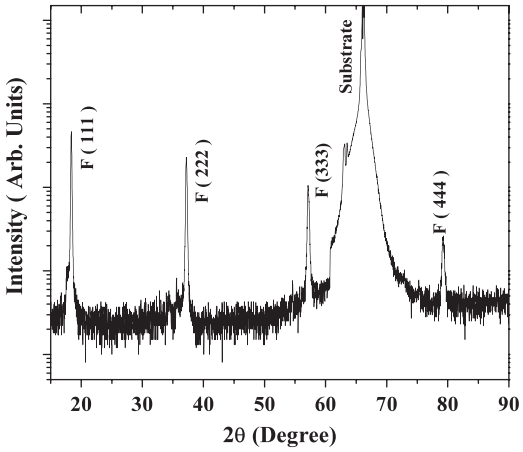

Figure 1. XRD pattern of Fe_3O_4 thin film on a GaAs(100) substrate grown by pulsed laser deposition. The film peaks are indicated by F and the reflection planes are indicated in parentheses.

by a stylus profilometer (Ambios, USA). These films were characterized by x-ray diffraction (Rigaku, Japan), and magnetization measurements. The electronic state of the iron ions and the presence of any other phase in the film were examined by core level x-ray photoelectron spectroscopy (Omicron-EA 125) using an Al Kα (1486.6 eV) radiation source. The spectral resolution of the spectrometer is 0.8 eV. Electrical and magnetic transport measurements were performed using a physical property measurement system (PPMS-Quantum Design, USA) by the standard four-probe method. The room-temperature magnetic hysteresis behavior of these thin films was examined using the vibrational sample magnetometer (VSM) technique (Lakeshore, Model 7401).

3. Results and discussions

The structure of the film was examined by XRD using Cu Kα radiation in θ–2θ geometry. We observed that films are highly oriented along the (111) direction with cubic structure (figure 1). The lattice parameter of the film, as calculated from the XRD pattern, is found to be 8.370 Å, which is close to the bulk lattice parameter (8.393 Å). It is recalled here that Lu *et al* [12] observed the epitaxial growth of Fe_3O_4 on a GaAs(100) substrate with an epitaxial relation of $Fe_3O_4(100)\langle 011\rangle \parallel GaAs(100)\langle 010\rangle$. Other reports such as Watts *et al* [14] and Kennedy *et al* [15] suggested the (111) preferred oriented growth of the film, as observed in the present study. However, Watts *et al* detected the minor contribution of other planes in their films. Whereas, Kennedy *et al* [15] suggested the possibility of some amorphous unoxidized iron at the interface of the film and substrate, since they used an iron target for ablation in the presence of a O_2 background for reactive deposition of Fe_3O_4. One possible reason for the (111) orientation of the Fe_3O_4 film on the GaAs(100) substrate may be that the (111) oriented Fe_3O_4 surface is the most energetically favorable one since the $\langle 111\rangle$ direction has the highest areal atomic density in the Fe_3O_4 spinel crystal structure [16]. It is noted here that in the present case the lattice mismatch between the film and substrate materials is very large, therefore, the growth orientation will be determined by the thermodynamically stable state having minimum internal energy. This is further confirmed by our very recent study [11] of pulsed laser deposited Fe_3O_4 films on Si substrates, where we have shown that the films are (111) orientated, independent of the Si substrate orientations.

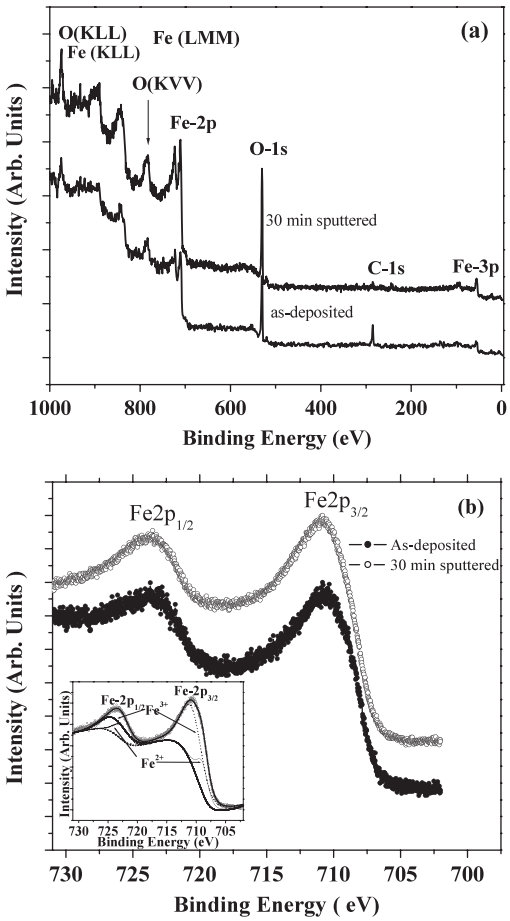

Figure 2. (a) Survey scan and (b) Fe 2p core level x-ray photoelectron spectra of as-deposited and 0.5 keV Ar^+ ion sputtered (30 min) Fe_3O_4 thin film on a GaAs(100) substrate grown by pulsed laser deposition. The inset in (b) shows the representative fitted spectra of the Fe 2p core level.

Since the lattice parameters of Fe_3O_4 (0.8396 nm) and γ-Fe_2O_3 (0.8342 nm) are very close to each other, the XRD pattern cannot distinguish between these two phases of iron oxide. To confirm the growth of the Fe_3O_4 film, the sample was characterized by x-ray photoelectron spectroscopy (XPS). We sputtered the film to remove the surface contamination and to understand the chemical state of iron deep inside the film. Sputtering was performed at a very low energy (500 eV) of Ar^+ ions so that it does not influence the composition of the film. In figure 2(a) we show the survey scans of as-deposited and 30 min sputtered films. It is evident that the as-deposited film has a small surface contamination of carbon, which is removed by sputtering. The XPS spectrum of the sputtered film has peaks corresponding to iron and oxygen. For the analysis of chemical compositions, the narrow scans were recorded for Fe and O core levels. In figure 2(b) we show the Fe 2p core level spectra of the as-deposited and 30 min sputtered film recorded in the binding energy (BE) range of 731–703 eV. These spectra were normalized with maximum intensity and shifted up side vertically for the sake of clarity. Because of the surface contamination in the as-grown film, we observe a less intense spectrum but after etching the film with Ar^+ ions, the intensity of the Fe 2p core level improves. From

figure 2(b), we observe that the Fe $2p_{1/2}$ and $2p_{3/2}$ peaks situated at around 711 and 724 eV are broadened due to the existence of both Fe^{2+} and Fe^{3+} ions. The Fe $2p_{3/2}$ and Fe $2p_{1/2}$ binding energies for Fe^{2+} and Fe^{3+} were determined by fitting the spectral line shapes to a convolution of Gaussian and Lorentzian functions (inset of figure 2(b)). The representative spectrum of the 30 min sputtered sample is shown in the inset of figure 2(b). The measured Fe $2p_{3/2}$ (Fe $2p_{1/2}$) binding energy is 709.2 eV (722.4 eV) for Fe^{2+} and 711.1 eV (724.5 eV) for Fe^{3+}. These values match the literature values very well [18]. From these fitted parameters we have calculated the Fe^{3+}/Fe^{2+} ratio, which comes out to be 2:1 as expected for Fe_3O_4. Since the binding energy position of the satellite of Fe $2p_{3/2}$ for different Fe oxidation states +2 or +3 occurs at 715 or 719 eV respectively, the corresponding satellite structure can be used to provide information about the presence of FeO or γ-Fe_2O_3. Fe_3O_4 being the mixed state of FeO and Fe_2O_3, its spectra has a smeared out unresolved structure in this energy range [19–21]. The features of the core level confirm the presence of Fe_3O_4 phase in the film and the absence of any other phase of iron oxide. Similar spectra are obtained for the films etched for longer duration, confirming the Fe_3O_4 phase deep inside the film as well.

After ensuring the structure and single-phase nature of Fe_3O_4 film, the resistivity measurement (ρ–T plot) was performed using the standard four-probe method down to 66 K (figure 3(a)). We notice that at 122 K, resistance increases sharply as we lower the temperature, a signature of the disorder to order transition. However, the transition is not that sharp as generally observed for bulk samples. The room-temperature resistivity value of the film (10 mΩ cm) is higher than the single-crystal bulk sample (4 m Ω cm). The higher value of resistivity and a rather broader transition can be attributed to the incoherent growth of the films resulting from a huge lattice mismatch between the films and the substrates. The activation energy of the film is calculated using the Arrhenius equation $\rho_H = \rho_0 \exp(-E_g/k_T)$ beyond the Verwey transition temperature in the temperature range 130–300 K. Figure 3(b) shows the plot between $\ln \rho$ and $1/T$. The plot shows a linear behavior in the studied temperature range and the activation energy is calculated to be 62.2 meV, which is close to the reported data for the Fe_3O_4 bulk value (58 meV) [22].

To understand the transport behavior below T_V, we fit our resistivity data with the Mott variable range hopping (VRH) model wherein conduction is considered by hopping between localized states, represented by expression [23] $\rho = \rho_0 \exp(T_0/T)^{1/4}$, where ρ_0 depends on phonon density and T_0 is the characteristic Mott temperature, a parameter determining the degree of disorder which is given by $k_B T_0 = 18\alpha^3/N(E)$, α being the inverse of localization length and $N(E)$ being the density of states at the Fermi level. In the upper inset of figure 3(b), we show the plot between $\ln \rho$ versus $(1/T)^{0.25}$ in the temperature range of 115 K to the lowest possible measured temperature 66 K. (Below 66 K, the film becomes too insulating to measure.) It is evident from the plot that $\ln \rho$ fits linearly with $(1/T)^{0.25}$ in the studied temperature range below T_V. From the slope of the linear fitting, we calculate the value of T_0 as 1.1×10^8 K, which is close to the earlier reported value (1.6×10^8 K) for epitaxial films of Fe_3O_4 on different substrates [10, 24]. However, the value of localization length ($1/\alpha$) is calculated to be 0.064 nm. This value of localization length is not physically meaningful. Therefore, considering the fact that below T_V, Fe_3O_4 has a charge ordered state, we used Shklovskii and Efros VRH model (SE-VRH) [25], which accounts for an electron–electron Coulombic interaction term. It is recalled here that there is a close similarity between the transport properties of charge ordered manganites and magnetite, since in both cases Coulomb interaction plays and important part in the hopping conduction of electrons. Hence, the SE model developed for the temperature dependence of resistivity in manganites by considering the theory of weak localization and VRH in the presence of a Coulomb gap should be applicable for Fe_3O_4 as well. The SE-VRH model is expressed by $\rho = \rho_0 \exp(T_0/T)^{1/2}$, where $T_0 = 2.8e^2\alpha/(4\pi k\varepsilon_0)$, k being the

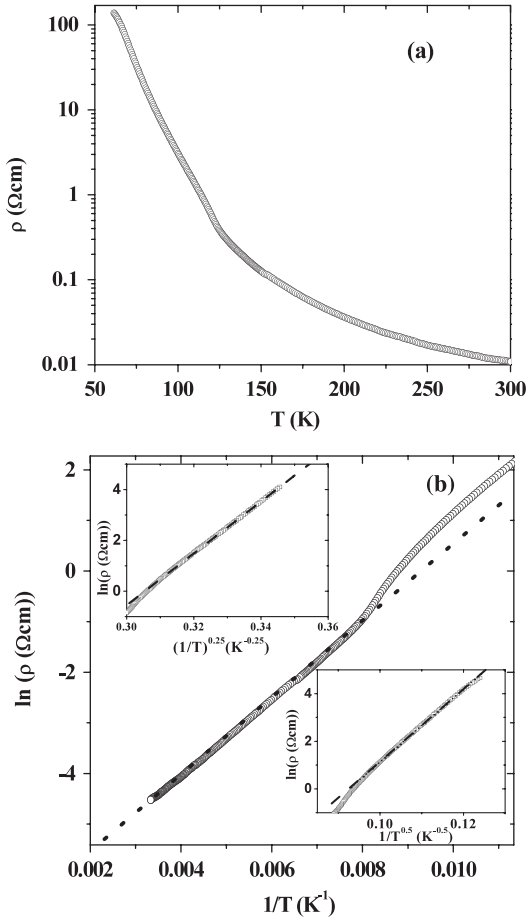

Figure 3. (a) Resistivity (ρ) as a function of temperature (T) for the Fe_3O_4 film; (b) plot between $\ln \rho$ versus $1/T$ with a linear fitting of the plot in the temperature range of 130–300 K; upper and lower insets show the plot between $\ln \rho$ versus $1/T^{0.25}$ and $\ln \rho$ versus $1/T^{0.5}$ with linear fitting in the temperature range of 115–66 K and 110–66 K, respectively.

dielectric constant of the material. The lower inset of figure 3(b) shows the plot between $\ln \rho$ versus $(1/T)^{0.5}$ in the temperature range of 110 K to the lowest possible measured temperature 66 K. The slope of the linear fitting in the plot yields $T_0 = 23\,440$ K. Using this value of T_0, we estimate the coherence length $(1/\alpha)$ to be equal to $\sim$2 nm, which is almost seven times the distance between the nearest neighborhood hopping distance between Fe^{2+} and Fe^{3+} ions at octahedral B sites of Fe_3O_4. This value of coherence length, as calculated from the SE-VRH model, is physically reasonable. Therefore, it seems that the SE-VRH model fits for the Fe_3O_4 film below $\sim 0.9T_V$ down to a measureable temperature of $\sim 0.5T_V$.

Now if we consider that below T_V the transport behavior shows SE-VRH type behavior then, the SE-VRH energy (Δ) should be equal to the Coulomb soft gap (U) occurring because of strong electronic correlation. To validate this point, we calculate Δ using the formula $\Delta = k_B\sqrt{(T_C T_0)}$, as derived from the SE-VRH model. Here T_C is the material's characteristic temperature, where the transition from nearest neighbor thermally activated hopping transforms into SE-VRH type hopping. In our study we consider T_C as equal to 110 K, which is the

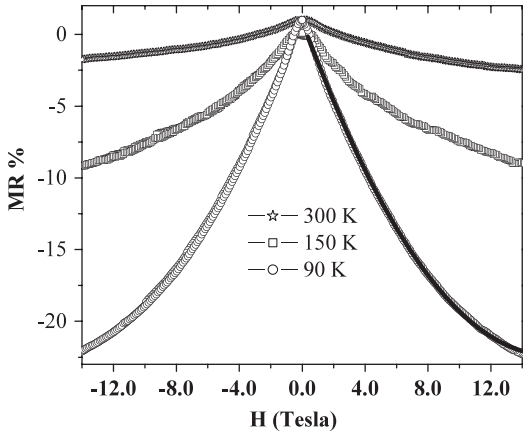

Figure 4. Field dependence of magnetoresistance (MR%) of Fe_3O_4 thin film on a GaAs(100) substrate grown by pulsed laser deposition at temperatures 90, 150, and 300 K.

maximum temperature for SE-VRH behavior. Using the calculated values of T_0 and T_C from the graph, we estimate $\Delta = 0.138$ eV. U can be calculated using the standard electrostatic relation $U = e^2/(4\pi\varepsilon_0 R_{avg})$, where R_{avg} is the average distance between hopping sites [26]. Taking the R_{avg} value to be 10 nm as calculated from the Hall measurement [27] and putting the respective values of T_0, e and ε_0, we obtain U as equal to 0.144 eV. The observed values of U and Δ are very close to each other, suggesting the applicability of the SE-VRH model below T_V in the present study. Earlier reports suggested Mott VRH type conduction behavior below T_V either in single-crystal or epitaxial films. We believe that in our study though the Mott VRH model fits well, SE-VRH behavior is more justified, given the fact that our films are not epitaxial but well oriented. Since in the present study the grain density would be larger than the epitaxial films, the transport behavior should occur via tunneling across the interface of two adjacent grains, which would provide a linear behavior between $\ln \rho$, and $(1/T)^{0.5}$ [28].

Figure 4 shows the magnetoresistance (MR%) behavior with magnetic field at different temperatures (90, 150, and 300 K), MR% is defined as $(R_H - R_0) * 100/R_0$. The magnetic field was applied perpendicular to the film plane. It may be seen that MR% is higher below T_v than the room-temperature value. We fit our MR data with expression $\rho_H = \rho_0[1 + \alpha H + \beta H^2]$, which has earlier been used for (111) oriented epitaxial thin films of Fe_3O_4 deposited on a sapphire substrate [10]. The MR data at all three temperatures fit very well to this form. At 90 K temperature the values of α and β are $0.0108T^{-1}$ and $3.1 \times 10^{-3}\ T^{-2}$ respectively. Ogale *et al* explained the similarity of the field dependent behavior of magnetoresistance between magnetite and manganites in terms of the importance of a small polaron in the conductance behavior of these two systems.

In figure 5 we show the room-temperature magnetization hysteresis behavior of the film. It is evident from the figure that the film shows a clear magnetic hysteresis behavior with coercivity of 372 Oe at room temperature. The magnetization saturates at a field value of 0.3 T with saturation magnetization (M_S) value close to 470($\pm$20) emu cm^{-3}, which is slightly lower than the single-crystal saturation value (480 emu cm^{-3}) [15]. The observed behavior suggests the room-temperature ferrimagnetic behavior of the film. In the earlier report, Kennedy *et al* observed a higher M_S value of 730 emu cm^{-3} in their Fe_3O_4 film on the GaAs substrate, which they accounted for by the presence of metallic Fe rich regions within the film. The minor deviation of the M_S value from that of the single crystal may be because of the presence of

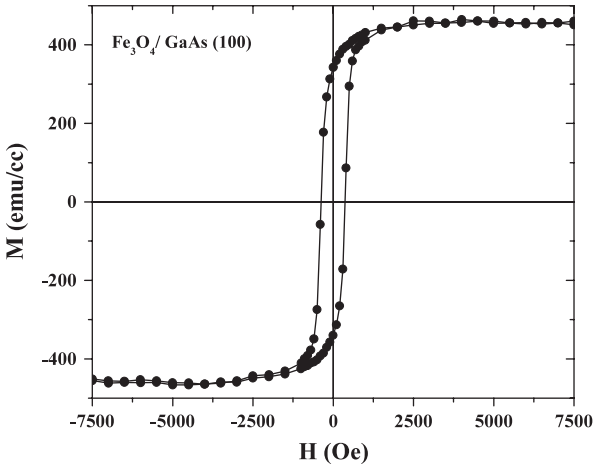

Figure 5. M versus H plot at 300 K of Fe_3O_4 film on a GaAs(100) substrate.

growth related defects in the film. It is known that epitaxial Fe_3O_4 films grown on a single-crystal MgO substrate possess a high density of anti phase boundary (APB) defects arising because of the double lattice parameter of Fe_3O_4 (8.3967 Å) as compared to that of the MgO substrate (4.213 Å) and lower symmetry of Fe_3O_4 compared to MgO. The consequence of these APB defects brings in the abnormal electrical and magnetic properties of Fe_3O_4, in particular the non-saturation of magnetization even at high field. The presence of APBs and the related effects are also known to occur in polycrystalline films of Fe_3O_4 grown on silicon substrates. In the present study the magnetization result ostensibly implies that our film is free from APB defects or has a lower density of such defects. However, we need a more plausible experimental verification in this regard.

4. Conclusions

In conclusion, we have successfully grown Fe_3O_4 thin film on a single-crystal GaAs(100) substrate using the pulsed laser deposition technique from a α-Fe_2O_3 target. These films are (111) oriented and single-phase, as confirmed by x-ray diffraction and x-ray photoelectron spectroscopy, respectively. These films also show a characteristic Verwey transition at 122 K. The electrical transport behavior of the films below T_V shows SE-VRH type behavior while above T_V it is of thermally activated type. The magnetization data reveal the room-temperature ferrimagnetic behavior of the film with saturation magnetization close to the bulk value.

Acknowledgments

The authors are grateful to Dr P Chaddah and Professor A Gupta for encouragement and acknowledge Dr V Ganesan for providing access to magnetoresistance measurements. We also thank Shailja Tiwari for her help in the sample preparation. One of us (RP) would like to acknowledge CSIR, N. Delhi for the financial support.

References

[1] Wolf S A, Awschalom D D, Buhrman R A, Daughton J M, von Molnár S, Roukes M L, Chtchelkanova A Y and Treger D M 2001 *Science* **294** 1488

[2] Versluijs J J, Bari M A and Coey J M D 2001 *Phys. Rev. Lett.* **87** 026601
[3] Zutic I, Fabian J and Das Sarma S 2004 *Rev. Mod. Phys.* **76** 323
[4] Verwey E J W 1939 *Nature* **144** 327
[5] Margulies D T, Parker F T, Rudee M L, Spada F E, Chapman J N, Aitchison P R and Berkowitz A E 1997 *Phys. Rev. Lett.* **79** 5162
[6] Arora S K, Sofin R G S and Shvets I V 2005 *Phys. Rev.* B **72** 134404
[7] Eerenstein W, Palstra T T M, Saxena S S and Hibma T 2002 *Phys. Rev. Lett.* **88** 247204
[8] Kale S, Bhagat S M, Lofland S E, Scabarozi T, Ogale S B, Orozco A, Shinde S R, Venkatesan T and Hannoyer B 2001 *Phys. Rev.* B **64** 205413
[9] Phase D M, Tiwari S, Prakash R, Dubey A, Sathe V G and Choudhary R J 2006 *J. Appl. Phys.* **100** 123703
[10] Ogale S B, Ghosh K, Shrama R P, Greene R L, Ramesh R and Venkatesan T 1998 *Phys. Rev.* B **57** 7823
[11] Tiwari S, Choudhary R J, Prakash R and Phase D M 2007 *J. Phys.: Condens. Matter* **19** 176002
[12] Lu Y X, Claydon J S and Xu Y B 2004 *Phys. Rev.* B **70** 233304
[13] Watts S M, Boothnan C, van Dijken S and Coey J M D 2005 *Appl. Phys. Lett.* **86** 212108
[14] Watts S M, Boothnan C, van Dijken S and Coey J M D 2004 *J. Appl. Phys.* **95** 7465
[15] Kennedy R J and Stampe P A 1999 *J. Phys. D: Appl. Phys.* **32** 16
[16] Preisler E J, Brooke J, Oldham N C and McGill T C 2003 *J. Vac. Sci. Technol.* B **21** 1745
[17] Lu Y X, Claydon J S and Xu Y B 2004 *J. Appl. Phys.* **95** 7228
[18] Barbieri A, Weiss W, Van Hove M A and Somorjai G A 1994 *Surf. Sci.* **302** 259
[19] Ruby C, Humbert B and Fusy J 2000 *Surf. Interface Anal.* **29** 377
[20] Gao Y and Chambers S A 1997 *J. Cryst. Growth* **174** 446
[21] Fujii T, De Groot F M F, Sawatzky G A, Voogt F C, Hibma T and Okada K 1999 *Phys. Rev.* B **59** 3195
[22] Kazlowaski A, Rasmussen R J, Sabol J E, Metacalf P and Honig J M 1993 *Phys. Rev.* B **48** 2057
[23] Mott N F and Davies E A 1979 *Electron Process in Noncrystalline Materials* (Oxford: Charendon)
Mott N F 1990 *Metal–Insulator Transitions* (London: Taylor and Francis)
[24] Gong G Q, Gupta A, Xiao G, Qian W and Dravid V P 1997 *Phys. Rev.* B **56** 5096
[25] Shklovskii B I and Efros A I 1984 *Electronic Properties of Doped Semiconductors* (Berlin: Springer)
[26] Chen X J, Zhang C L, Gardiner J, Sarrao L and Almasan C C 2003 *Phys. Rev.* B **68** 64405
[27] Siemons W J 1970 *IBM J. Res. Dev.* **14** 245
[28] Liu H, Jiang E Y, Bai H L, Zheng R K and Zhang X X 2003 *J. Phys. D: Appl. Phys.* **36** 2950